Simulation of an ammonia-water absorption cycle using exchanger effectiveness

Simone Braccio, Hai Trieu Phan, Mathilde Wirtz, Nicolas Tauveron, Nolwenn Le Pierrès

Simulation of an ammonia-water absorption cycle using exchanger effectiveness

Simone Braccio[1,2], Hai Trieu Phan[1], Mathilde Wirtz [1,2], Nicolas Tauveron[1], Nolwenn Le Pierrès[2,*]

[1] Université Grenoble Alpes, CEA, Liten, Campus INES, 73375 Le Bourget du Lac, France

[2]*LOCIE, Université Savoie Mont Blanc, CNRS UMR5271, Savoie Technolac, 73370 Le Bourget Du Lac, France*

**Corresponding author: nolwenn.le-pierres@univ-smb.fr*

ARTICLE INFO

Keywords:
Absorption chiller
Ammonia/Water mixture
Numerical Simulation
Exchanger effectiveness

HIGHLIGHTS

- NH_3/H_2O absorption chiller modeling based on exchanger effectiveness
- Tuning of the numerical model on experimental results
- Comparison of simplified and effectiveness-based modeling
- Characterization of performance for changing operating conditions
- Parametric study changing the size of components

ABSTRACT

This paper presents the numerical simulation of an efficient ammonia-water single-stage absorption chiller integrating a new combined desorber, able to produce and purify the refrigerant vapor. An experimental campaign was conducted on the pilot plant by varying the main operating parameters, namely the temperatures of external sources and the mass flow rate of the working fluid. Direct experimental measures were analyzed and indirect calculation of other physical quantities was used for tuning of the numerical models.

First, a simplified model of the cycle was developed, based on fixed effectiveness and pinch temperatures. Absolute values and tendencies outside nominal working conditions were not sufficiently accurate to predict the performance of the cycle even at the small scale, so more accurate modeling was undertaken. Accordingly, components were characterized by effectiveness, modeled using three operating parameters: the Jakob number (Ja), the number of transfer units (NTU) and the energetic ratio (R_{en}). The small average errors for calculated effectiveness confirm that these parameters are well suited for the application studied. Global cycle model results showed errors compared to experimental results below 6 % for the COP and 15 % for the cooling power output. The tuned model was used to perform a parametric analysis on the dimension of the components, highlighting the performance improvements/reductions obtainable by increasing/decreasing their size. The use of dimensionless parameters makes this approach well suited for analysis at larger scales of industrial interest, the development of more complex or combined cycles as well as to perform techno-economic or exergo-economic analysis.

Nomenclature

cp	heat capacity	[kJ. kg^{-1}.K^{-1}]
h	enthalpy	[kJ.kg^{-1}]
Ja	Jakob number	[-]
K	overall heat transfer coefficient	[W.m^{-2}.K^{-1}]
L	latent heat	[kJ.kg^{-1}]
$\dot{m}$	mass flow rate	[kg.s^{-1}]
P	pressure	[bar]
$\dot{Q}$	power	[kW]
R	ratio	[-]
S	surface	[m^2]
T	temperature	[K]
x	liquid ammonia mass fraction	[-]
ΔT	pinch of temperature	[°C]
ε	effectiveness	[-]
ρ	density	[kg.m^{-3}]

Acronyms

COP	thermal coefficient of performance
NTU	number of transfer units
HTF	heat transfer fluid

Indices

a	absorber
c	condenser
d	desorber
en	energetic
e	evaporator
HTF	heat transfer fluid
id	ideal
i	inlet
int	intermediate
liq	liquid
LF	limiting fluid
mass	mass
max	maximum
min	minimum
NLF	non-limiting fluid
o	outlet
ref	refrigerant
sat	saturation
shx	solution heat exchanger
sol	solution
sp	poor solution
species	species
sub	subcooler
sr	rich solution
th	thermal
vap	vapor

*Corresponding author.
E-mail address: nolwenn.le-pierres@univ-smb.fr (N. Le Pierrès)

1. Introduction

Due to the ever-increasing global demand for energy and growing concern about environmental issues and climate change, the scientific community has focused its attention on the search for new and efficient energy conversion technologies based on renewable sources [1][2][3]. All sectors are involved from power production and transport to heating and cooling [4][5]. The tripling of global energy demand for cooling in residential buildings [6] between 1990 and 2016 shows that this end use is growing much faster compared to other uses, resulting in an ever increasing demand for electricity. Cooling is mainly delivered using conventional technologies such as air conditioners which supply about 75 % of the world cooling demand. Worldwide there are around 1.6 billion cooling systems with a total consumption of over 2000 terawatt hours (TWh) of electricity per year [6], nearly two and a half times the total annual electricity consumption of Africa. A continuous increase in cooling systems globally is foreseen, with installed power expected to reach 3500 GW in 2050, i.e., four times the power installed in 2016.

Cooling systems based on recovery of waste energy and on thermal and photovoltaic solar energy consume less electricity resulting in fewer climate-changing emissions. Increased adoption of such systems is therefore key to improving the sustainability of cooling. In this context, absorption systems [7] are very well suited for the recovery of thermal energy as they replace the mechanical vapor compression of standard air conditioners by thermochemical compression. The circulation pump in such systems consumes a modest amount of electricity and can use any type of thermal source as the main driver, notably renewable sources (e.g., solar) or waste heat. In addition they use fluids that are not harmful to the environment [8] [9] [10], require low maintenance due to the absence of moving parts (except for the pump) and they produce very little noise and vibration. However, these systems are bulky and heavy and are more costly than traditional vapor compression systems. Research is needed to improve their performance and compactness as well as to reduce their cost.

Absorption systems can be divided into three categories based on the cycle arrangement: single stage, half-effect and multi-effect. In terms of cost, low driving temperatures and simplicity in the single-effect cycle proved to be the most advantageous and is therefore the most commercially available. Many absorption pairs have been investigated [11], but two pairs are more commonly encountered: water-lithium bromide and ammonia-water. The first pair generally allows higher COP to be reached while the latter allows the production of cooling at negative temperatures and development of innovative new cycles for combined production of cooling and electricity [12].

The object of this work is the study of a small capacity ammonia-water single stage absorption chiller of nominal desorber power of 10 kW and cooling power of 7 kW. The pre-industrial prototype was developed at CEA INES starting in 2012 [13] with the goal of redesigning components to optimize their performance and test innovative cycle architectures [14]. In addition, experimental tests on the pilot plant serve as a valuable source of data for the development and validation of numerical models [15].

Appropriate modeling is of fundamental importance for performance evaluation, characterization and optimization of a system. Existing models can be divided into three categories depending on their nature: physical, semi-empirical, with some degree of physical insight, and black box or empirical, when no physical insight is necessary and the model describes a dataset of experimental results [16]. Black box methods include multivariate polynomial regression and artificial neural network models [17]. Semi-empirical models were proposed as an alternative by Gordon [18] and Ziegler [19] who adapted the characteristic equation method to account for the fact that predicted cooling capacity deviates considerably from the linear behavior, particularly at high temperatures. Despite the increased accuracy of these models, the underlying physics of cycle functioning are concealed, and the calculated performance can deviate considerably from experimental performance, especially outside nominal conditions. A more accurate approach is to implement semi-empirical effectiveness in a physical model considering heat and mass transfer processes separately [16]. Physical models provide the best results in steady state conditions but need access to the physical properties of fluids [15]. Several correlations have been proposed for the ammonia-water mixture. Thorin [20] compared the saturation properties predicted by the correlations of Stecco and Desideri [21], Ibrahim and Klein [22] and Tillner-Roth and Friend [23], showing that at low temperatures they all give very similar results and that the difference is not significant for performance calculation at low temperatures (below 250 °C).

This paper develops a model of the absorption machine as a whole based on semi-empirical models of the individual components tuned using experimental data. The component models are then integrated in a physical model of the cycle, capable of predicting its performance, and taking into account the size and architecture of the specific application. Hence, the first step was to carry out an experimental campaign changing the main operating parameters. Experimental results were analyzed critically, excluding unreliable points, to be able to obtain an accurate database for numerical model adjustment. Initially a simplified physical model using fixed pinch temperatures was developed serving as a term of comparison for more detailed models. Then, a more detailed model of the pilot plant was developed based on thermal, mass and species semi-empirical effectiveness for each exchanger. Heat exchanger effectiveness is often characterized using dimensionless parameters like the number of transfer units (NTU) and the energetic ratio (R_{en}) between the maximum and minimum heat capacity of the two fluids. In the case of absorption machines, the absorber and the desorber represent two atypical heat exchangers in

which sorption processes also take place, making it necessary to include another parameter, the Jakob number (Ja) for their characterization. The experimental behavior of each exchanger was characterized using appropriate effectiveness, and the various correlations developed to model them were integrated in the physical model of the cycle and compared to experimental results. Finally, the model provided deep insight into the functioning of the system, and was used to perform a parametric analysis on component size and its effect on cycle performance.
The aim of this paper is to propose a modeling method for absorption machines able to give reliable information on the performance also when changing the plant size. This is particularly useful, for example, to evaluate the scale-up of the technology, help designing the relative size of components of the cycle and perform techno-economic or exergo-economic analysis. Finally, this type of modeling can be very useful in the development of combined cooling and power cycles, for which the water-ammonia couple is particularly suitable.

2. Description of the cycle

2.1. Cycle architecture

The absorption chiller under investigation is shown schematically in **Fig. 1**. The functioning is that of a classical single-stage ammonia-water absorption machine. On the solution circuit loop, a first line of solution rich in ammonia circulates from the absorber to the desorber and is pressurized by a pump. A second line comprising an expansion valve returns the poor solution to the absorber. An economizer, the solution heat exchanger, preheats the rich solution with the heat from the poor solution leaving the desorber where a power supply $\dot{Q}_d$ at high temperature allows the desorption of vapor mainly consisting of ammonia from the solution. Since both ammonia and water are volatile substances, a vapor rectification process is needed at the outlet of the desorber to remove the remaining water evaporated with the refrigerant. This is normally done with a rectifier, a component placed at the desorber exit ensuring good vapor purification and preventing potential COP reductions over 30 % due to water in the evaporator [24]. Here, the use of the rectifier is no longer needed due to the integration of a new desorber in the loop, as developed by Wirtz et al [25]. This new component performs an internal purification of the exiting vapor through partial reabsorption by the entering rich solution, allowing a very high ammonia concentration to be reached in the vapor and avoiding the need for rectification.

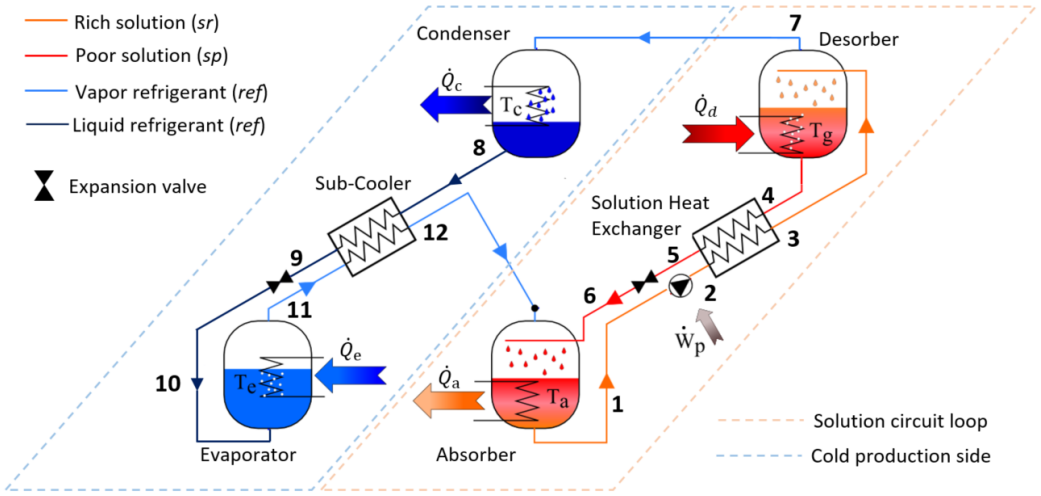

Fig. 1. Schematic of the absorption chiller.

On the cold production side, the refrigerant vapor is condensed through the exchange of thermal power $\dot{Q}_c$ with an intermediate temperature source. Before cooling the low temperature heat source at the evaporator by absorbing power $\dot{Q}_e$, the fluid is expanded in a valve to reach low pressure. A sub-cooler is used to pre-cool the ammonia before it expands by transferring heat to the refrigerant vapor coming out of the evaporator. The vapor flow is finally absorbed in the poor solution due to cooling by an intermediate temperature source (the same used in the condenser) to which a power $\dot{Q}_a$ is transferred in the absorber.

2.2. Experimental pilot plant

The study is based on an existing absorption chiller device in the development phase at CEA INES [13]. The prototype (shown in **Fig. 2**) is a thermally driven single-effect ammonia-water absorption chiller of 7 kW cooling capacity designed for the development of new components and testing of innovative combined cooling and power architectures in solar cooling applications.

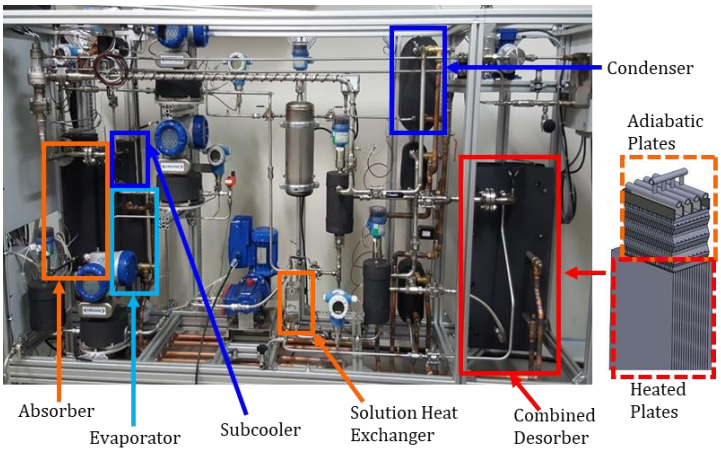

Fig. 2. Picture of the prototype of the NH_3/H_2O based cogeneration cycle [26].

Given that the ammonia-water mixture is corrosive to common materials, great attention was paid to all materials in contact with the fluid, using stainless steel and EPDM or PTFE for seals and membranes. The chiller is composed of six plate heat exchangers, the four main ones being external heat and mass exchangers: a desorber, absorber, evaporator and condenser, that exchange heat with an external Heat Transfer Fluid (HTF), here water. Two internal heat exchangers, a solution heat exchanger and a subcooler are needed to improve the performance of the cycle and are shown in **Fig. 1**.

As explained previously, the desorber integrated in the loop is a combined component (**Table 1**), based on falling film technology. This heat exchanger is composed of a lower part where vapor is generated exchanging heat with the hot source, and an adiabatic upper part allowing the purification of the vapor generated by partial reabsorption of the latter in the ammonia-water solution entering the exchanger. The combination of the heated and adiabatic sections enables replacing two plate heat exchangers used for the desorber and the rectifier as well as two associated phase-separation bottles with only one component, thus helping to reduce costs and overall dimensions. In fact, the high purity of the ammonia vapor at the desorber exit eliminates the need for further purification, making this solution particularly interesting in terms of compactness and performance [27].

Table 1

Dimensions of the desorber [25].

	Heated Plates (Bottom)	Adiabatic Plates (Top)
Plate length	320 mm	100 mm
Plate width	150 mm	90 mm
Plate thickness	6 mm	0.8 mm
Number of plates	14	28
Total surface	0.67 m^2	0.5 m^2

The other key component of the cycle, the absorber, is a falling film gasketed plate-and-frame commercial heat exchanger with corrugated plates, previously studied by Triché et al. [28]. The geometry of the absorber as well as that of the other stainless steel corrugated plate heat exchangers is given in **Table 2**.

Table 2

Dimensions of the heat exchangers of the cycle.

	Absorber	Condenser	Evaporator	Solution Heat Exchanger	Subcooler
Plate width	96 mm	111 mm	111 mm	72 mm	72 mm
Plate length	668 mm	310 mm	310 mm	187 mm	187 mm
Plate thickness	0.5 mm	0.5 mm	0.5 mm	0.5 mm	0.5 mm
Number of plates	16	40	24	25	20
Total surface	0.89 m^2	1.29 m^2	0.75 m^2	0.31 m^2	0.24 m^2

The solution pump being the major electricity consuming component of the chiller, special attention was paid to its specifications with regard to hydraulic, environmental, user and electrical constraints as explained in [13].
Since the liquid solution entering the pump comes from the absorber, its temperature is relatively close to saturation. If some frictional heating occurs, there is a risk of desorption around the moving parts, which can severely alter lifespan. These considerations lead to the selection of a diaphragm pump as the solution pump.
Two actuated expansion valves are present in the loop, one before the evaporator, charged with controlling the temperature glide during the evaporation process, and the other before the absorber on the poor solution line.
The ammonia-water absorption chiller is fully instrumented (**Fig. 3**). Measures of temperature (with T-type thermocouples for working fluid and with a platinum resistance thermometer for heat transfer fluid), density and mass flow rate (with Coriolis flow meters) and pressure are available at the inlet and the outlet of the main components. With this instrumentation, it is possible to calculate both the mass fraction in the different lines of the circuit and produce energy balances for each component. The chiller sensors are described in **Table *3*.**

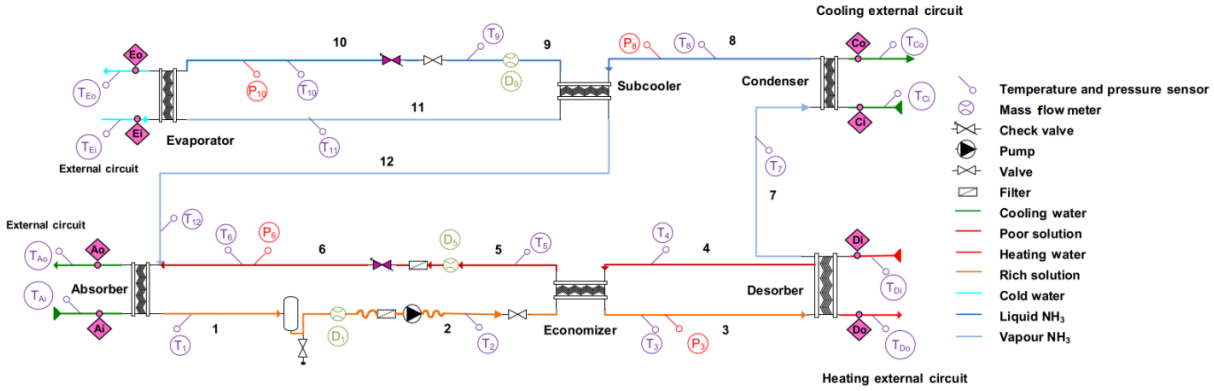

Fig. 3. Schematic view of the machine.

Table 3

Sensor number and measurement characteristics.

Sensor Type	Number	Uncertainty (±)
P-Type cooling or heating fluid temperature	8	0.15 K
T-type refrigerant and solution temperature	12	0.18 K
Low pressure (0-10 bar)	2	0.4 %
High pressure (0-20 bar)	2	0.8 %
Coriolis flow meter (Mass flow rate and density)	3	0.3 % - 2.3 kg/m^3

External heat transfer fluids (HTF), temperatures and mass flow rates, rich solution mass flow rate and temperature glide in the evaporator are the only control parameters available. They are used to modify the operating conditions of the chiller to perform the tests necessary for the tuning of numerical models. Design values and variability range for these parameters are shown in **Table 4**.

Table 4

Nominal point and operating range of components.

		Evaporator	Condenser	Absorber	Desorber	Pump
Temperature [°C]	Minimal	10	22	22	80	-
	Nominal	18	27	27	95	32
	Maximal	22	30	30	106	50
Pressure [bar]	Minimal	5	11	5	11	-
	Nominal	7	12	7	12	7/12
	Maximal	8	14	8	14	5/20
HTF and pump mass flow rate [kg/h]	Minimal	200	200	200	200	-
	Nominal	1100	1200	1200	1600	150
	Maximal	1200	1300	1300	1800	250
Power [kW]	Nominal	7	7	9	10	0.55

3. Experimental campaign

In order to tune the numerical model of the absorption chiller, an experimental campaign was carried out with the main goal of characterizing the behavior of the pilot plant. The experimental tests were conducted varying the main operating parameters that influence cycle performance, namely the temperature of the sources and the mass flow rate of the rich solution circulating in the loop. Stable operating conditions were reached for each test point and the quantities measured were averaged over the period of steady functioning, to obtain the time-averaged points shown in **Table 5**. The interval of variation was 80-106 °C for the desorber temperature, 600-1800 kg/h for the desorber HTF mass flow rate, 22-30 °C for the intermediate source temperature T_{int}, 80-110 kg/h for the rich solution mass flow rate and 10-22 °C for the HTF temperature entering the evaporator. The temperature glide in the evaporator was kept constant in all the tests at 5 °C as well as the mass flow rate of the other components' HTF.

Table 5

Experimental campaign matrix.

Point	High temperature source [°C]	Desorber HTF mass flow rate [kg/h]	Intermediate temperature source [°C]	Low temperature source [°C]	Rich solution mass flow rate [kg/h]
1	**106.1**	1600	26.9	17.7	100
2	**102.2**	1600	27.2	17.8	100
3	**100.2**	1600	27.0	17.8	100
4	**98.2**	1600	27.1	17.8	100
5	**95.2**	1600	27.0	17.8	100
6	**92.2**	1600	27.0	17.8	101
7	**90.2**	1600	27.0	17.8	101
8	**85.2**	1600	26.9	17.7	99
9	**80.2**	1600	27.0	17.8	100
10	95.2	**1800**	26.7	17.7	100
11	95.2	**1600**	26.8	17.7	100
12	95.2	**1400**	26.7	17.7	99
13	95.1	**1200**	26.7	17.7	100
14	95.1	**1000**	26.7	17.7	99
15	95.0	**800**	26.6	17.7	99
16	94.9	**600**	26.7	17.7	99
17	95.2	1600	**30.2**	17.7	101
18	95.2	1600	**28.2**	17.7	101
19	95.2	1600	**26.2**	17.7	99
20	95.1	1600	**25.3**	17.7	100
21	95.1	1600	**22.5**	17.7	100
22	95.2	1600	27.0	17.7	**110**
23	95.2	1600	27.0	17.7	**105**
24	95.2	1600	27.0	17.7	**100**
25	95.2	1600	27.1	17.7	**95**
26	95.2	1600	27.1	17.7	**89**
27	95.2	1600	27.0	17.7	**85**
28	95.2	1600	27.1	17.7	**80**
29	95.2	1600	26.9	**21.7**	100
30	95.2	1600	27.1	**19.7**	99
31	95.2	1600	27.0	**17.7**	100
32	95.2	1600	27.0	**15.7**	100
33	95.2	1600	27.0	**13.7**	101
34	95.2	1600	27.0	**11.7**	100
35	95.2	1600	27.0	**9.8**	100

The power exchanged by each external heat exchanger is calculated through an energy balance on the HTF side knowing the temperature at the inlet and outlet of the exchanger and the HTF mass flow rate.

3.1. Ammonia concentration calculation

Experimental data lack the direct measures of concentration within the loop, which is very difficult to achieve and not practicable. These data are necessary for calculation of the thermodynamic properties of the mixture and characterization of the functioning of the evaporator, desorber, and absorber and therefore need to be deduced from other direct measures. Indirect evaluation of the concentration is possible, using the thermodynamic properties (*h, T, P*, etc.) of ammonia-water solution obtained from the Engineering Equation Solver, based on the mixture equation of state developed by Ibrahim and Klein [22]. The correlations are applicable for temperatures between 230 K and 600 K at equilibrium pressures between 0.2 and 110 bar with an average deviation of less than 5 % with respect to reported experimental data.

Ammonia concentration inside the loop can be calculated in several ways. For example, one possibility is to use the available measures of pressure and temperature together with the density measured by the Coriolis flowmeter on the rich and poor solution side (**Fig. 3**):

$$x_{sr} = x\,(T_1, P_6, \rho_1) \quad (1)$$

$$x_{sp} = x\,(T_5, P_3, \rho_5) \quad (2)$$

The values of ammonia concentration in the vapor refrigerant x_{ref} calculated with a mass balance on the desorber were often exceeding 1 for the test points and therefore this procedure was not retained. An alternative is to calculate the ammonia concentration of the refrigerant vapor from an energy balance formulated on either the condenser (Eq.(3)) or the evaporator (Eq.(4)):

$$\dot{Q}_c = \dot{m}_9 \cdot h\,(T_7, P_8, x_{ref}) - \dot{m}_9 \cdot h\,(T_8, P_8, x_{ref}) \quad (3)$$

$$\dot{Q}_{evap} = \dot{m}_9 \cdot h\,(T_{10}, P_{10}, x_{ref}) - \dot{m}_9 \cdot h\,(T_{11}, P_{10}, x_{ref}) \quad (4)$$

Knowing this value, the other two concentrations can be calculated either by assuming that the solution leaving the desorber is saturated liquid (Eq.(5) and Eq.(7)), or by performing an energy and mass balance on the desorber (Eq.(6)-(7)) or on the absorber (Eq.(8)-(9)):

$$x_{sp} = x_{liq,sat}\,(T_4, P_3) \quad (5)$$

$$\dot{Q}_d = \dot{m}_{ref} \cdot h\,(T_7, P_3, x_{ref}) + \dot{m}_{sp} \cdot h\,(T_4, P_3, x_{sp}) - \dot{m}_{sr} \cdot h\,(T_3, P_3, x_{sr}) \quad (6)$$

$$\dot{m}_{sr} \cdot x_{sr} = \dot{m}_{sp} \cdot x_{sp} + \dot{m}_{ref} \cdot x_{ref} \quad (7)$$

$$\dot{Q}_a = \dot{m}_{ref} \cdot h\,(T_{12}, P_{10}, x_{ref}) + \dot{m}_{sp} \cdot h\,(T_6, P_6, x_{sp}) - \dot{m}_{sr} \cdot h\,(T_1, P_1, x_{sr}) \quad (8)$$

$$\dot{m}_{sr} \cdot x_{sr} = \dot{m}_{sp} \cdot x_{sp} + \dot{m}_{ref} \cdot x_{ref} \quad (9)$$

The concentrations calculated with the different procedures were used to calculate the power exchanged by the working mixture in each exchanger and compared with the power exchanged by the HTF, considered to be the effective power exchanged by the component. Calculation of the refrigerant vapor concentration through an energy balance on the evaporator (Eq.(4)) and assuming the poor solution leaving the desorber to be saturated liquid (Eq.(5) and Eq.(7)), was found to have the smallest average error between the power calculated on the solution side and the HTF side. The average ammonia concentration in the vapor calculated in this way for the points of **Table 5** was 0.989, while the minimum was 0.982.

Power balance errors on components higher than 5 % between the power calculated on the solution side and on the HTF side were not accepted and points 17– 22- 33 -34-35 were discarded for the following numerical adjustment of coefficients as they were not considered to be sufficiently reliable. As a validation check, refrigerant ammonia concentration was used to calculate the saturated liquid pressure at the condenser outlet and evaporator inlet temperature which are used to model the high and low pressure in the loop [7]. A comparison with experimentally measured pressure shows a difference of less than 3 % for the high pressure and less than 1 % for the low pressure thus validating the use of this hypothesis in the model of the cycle. Knowledge of the ammonia concentration together with measures of temperature and pressure makes it possible to define the thermodynamic state of the fluid at every point of the loop and to calculate the experimental effectiveness of each exchanger as well as the dimensionless number used to model them, as shown in the following sections.

4. Numerical modeling of the cycle and parameter tuning

A simplified model is presented below in which the components are described by means of an average temperature pinch based on experimental tests for the external exchangers and constant effectiveness for the internal exchangers. Subsequently, a more detailed model is presented in which the functioning of the components is modeled using experimental effectiveness. For each test point, the experimental effectiveness of the components is calculated from experimental measures and a correlation is presented to model them using three dimensionless numbers: the energetic ratio R_{en}, the number of transfer units NTU and the Jakob number Ja. The effectiveness correlations are integrated in the model and tuned on experimental results. Finally, the results of the simplified model and the adjusted effectiveness model are compared.

4.1. Simplified model of the cycle

A simplified steady state numerical model of the absorption cycle previously introduced was developed based on the description in Herolds et al. [7] with respect to which only the specific differences due to the combined desorber are highlighted here. For each component, the energy and mass conservation equations were formulated. The parameters of each heat exchanger (pinch or effectiveness) were set based on the values assessed experimentally in order predict well the performance of the ammonia-water absorption prototype in the nominal operating point. It is assumed that the mixture is saturated at the outlet of desorber and condenser and at the inlet of the evaporator.

The desorber considered is a combined component that generates vapor and purifies it by exchanging heat with the liquid solution at the inlet. Therefore, in ideal conditions, the refrigerant vapor at the outlet reaches the same temperature as the solution at the inlet and its concentration is that of saturated vapor at the inlet temperature of the rich solution T_3:

$$x_{7,id} = x_{vap,sat}(T_3, P_3) \tag{10}$$

The conditions of the poor solution at the outlet can then be calculated through an energy balance on the desorber as explained previously. The performance of the absorber is modeled with a mass effectiveness $\varepsilon_{mass,a} = \dot{m}_{12}/\dot{m}_{12,max}$ fixed to 0.6 [28] and a temperature pinch between the HTF at the inlet and the rich solution at the outlet $\Delta T_a = T_{1} - T_{a,i}$ fixed to 5 °C. A fixed pinch of temperature of 5 °C is imposed between the inlet of the intermediate temperature HTF and the liquid refrigerant exiting the condenser ($\Delta T_c = T_8 - T_{c,i}$). The high pressure of the cycle is then determined as the saturated liquid pressure at the condenser outlet temperature T_8 and ammonia mass fraction x_8.
The evaporator performance is defined by the pinch between the HTF at the inlet and the refrigerant fluid at outlet ($\Delta T_e = T_{e,i} - T_{11}$) imposed equal to 5 °$C$ and a temperature glide between the inlet and outlet of the component ($\Delta T_{glide} = T_{11} - T_{10}$) also imposed equal to 5 °C. Knowing the refrigerant evaporator inlet temperature, the low pressure of the cycle can be determined as the saturated liquid pressure at T_{10} and x_{10}. The solution heat exchanger effectiveness $\varepsilon_{shx} = \dot{Q}_{shx}/\dot{Q}_{shx,max}$ is set equal to 0.8 and the subcooler effectiveness $\varepsilon_{sub} = \dot{Q}_{sub}/\dot{Q}_{sub,max}$ is set to 0.9. Details for the calculation of $\dot{m}_{12,max}$, $\dot{Q}_{shx,max}$ and $\dot{Q}_{sub,max}$ will be given in the following sections. Finally, no pressure drop or thermal dispersion is considered and the pump isentropic efficiency is set to 0.8 [13].

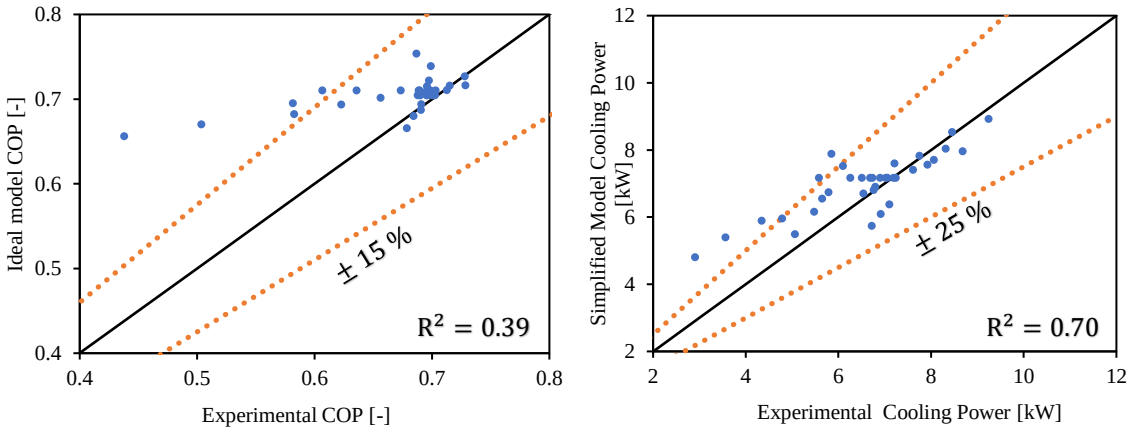

Fig. 4. Comparison of the simplified numerical model with experimental results.

The results of the simplified model are compared to the experimental measures in **Fig. 4**. The model of the cycle predicts the experimental results well at the operating point near the nominal conditions. Nevertheless, considering

fixed component effectiveness results in simulated points differing substantially from experimental for conditions other than nominal, with a frequent overestimation of performance. This highlights the need for more accurate modeling so the model can be used reliably for different applications and plant sizes. The development of a model based on variable semi-empirical effectiveness is therefore presented in the following paragraphs.

4.2. Experimental effectiveness model (ε-model)

With the goal of better describing the behavior of the machine, a more detailed steady state model was developed by introducing variable experimental effectiveness to describe the functioning of each heat exchanger. Also in this case, the assumption is made that the fluid is at saturation at the outlet of desorber and condenser and at the inlet of the evaporator. The efficiency of the pump is assumed equal to 0.8, expansion in valves is considered isenthalpic and pressure drops and thermal dispersions are neglected. The only inputs of the developed model are the control parameters of the pilot plant (HTFs temperatures and mass flow rates, rich solution mass flow rate and temperature glide in the evaporator).
Experimental effectiveness were calculated comparing the actual performance of exchangers with that of ideal components. Three dimensionless numbers were used in the modeling of the effectiveness: the energetic ratio R_{en}, the number of transfer units NTU and the Jakob number Ja [29]. R_{en} is defined as the ratio of the maximum power transferable to the non-limiting fluid over the maximum power transferable to the limiting fluid in the exchange:

$$\mathrm{R_{en}} = \frac{\max(\dot{\mathrm{Q}}_{\mathrm{HTF,max}}, \dot{\mathrm{Q}}_{\mathrm{sol,}})}{\min(\dot{\mathrm{Q}}_{\mathrm{HTF,max}}, \dot{\mathrm{Q}}_{\mathrm{sol,max}})} \tag{11}$$

The number of transfer units *NTU* is a dimensionless parameter characterizing the rate of heat transfer in counter-current exchangers. It is defined as the ratio of the product of the heat transfer coefficient K and the exchange S surface to the smallest heat capacity rate between the two fluids [30]:

$$\mathrm{NTU} = \frac{\mathrm{K \cdot S}}{(\dot{\mathrm{m}} \cdot \mathrm{Cp})_{min}} \tag{12}$$

The global heat transfer coefficient K considers both convective transfers between falling film and plate and between the HTF and plate and conduction across the absorber plate. For the external heat exchangers, the HTF side heat transfer coefficient is calculated with a correlation developed by the Heat Exchangers Research Group (GRETh) for corrugated plates with a Reynolds number value between 50 and 14,600 [28], while the convective heat transfer coefficient between the falling film and the plates is calculated with the Wilke's correlation [31]. For the solution heat exchanger correlations developed by the GRETh was used on both sides.

The Jakob number (Ja) is a dimensionless number defined as the ratio of the solution sensible heat to the latent heat released during the liquid vapor phase change:

$$\mathrm{Ja} = \frac{\rho_{\mathrm{sol}} \cdot \mathrm{cp_{sol}} \cdot (\mathrm{T_{HTF,i}} - \mathrm{T_{liq,sat}})}{\rho_{\mathrm{vap}} \cdot \mathrm{L}} \tag{13}$$

Where ρ_{sol}, $\mathrm{cp_{sol}}$ and L are the density, specific heat and latent heat of vaporization of the entering solution, $\mathrm{T_{HTF,i}}$ is the temperature of the HTF at inlet and $\mathrm{T}_{liq,sat}$ is the temperature of the saturated liquid at the inlet at the given pressure and concentration. The following sections show the definition of the effectiveness for each component and the semi-empirical correlations proposed for modeling them.

4.2.1. Desorber model

The performance of the desorber considered in the present study can be characterized using three effectiveness: thermal, mass and species [29]. These effectiveness relate the functioning of the desorber to that of an ideal one. In an ideal desorber, the vapor at the outlet reaches the same temperature $\mathrm{T_3}$ of the entering rich solution with which it exchanges heat, increasing its ammonia concentrations to that of saturated vapor at $\mathrm{T_3}$ (Eq. (14)). For fixed mass flow rate and thermodynamic conditions at the inlet, the minimum mass flow rate of poor solution $\dot{\mathrm{m}}_{4,min}$, the maximum mass flow rate of vapor $\dot{\mathrm{m}}_{7,max}$ and the maximum power exchanged by the ideal desorber $\dot{\mathrm{Q}}_{\mathrm{des,max}}$ are deduced from mass, species and energy balances and assuming the poor solution at the outlet to be saturated:

$$x_{7,id} = x_{vap,sat}\ (T_3, \mathrm{P_7}) \tag{14}$$
$$x_{4,id} = x_{liq,sat}\ (T_4, \mathrm{P_4}) \tag{15}$$

$$\dot{m}_3 = \dot{m}_{4,\min} + \dot{m}_{7,\max} \quad (16)$$

$$\dot{m}_3 \cdot x_3 = \dot{m}_{4,\min} \cdot x_{4,id} + \dot{m}_{7,\max} \cdot x_{7,id} \quad (17)$$

$$\dot{Q}_{d,\max} = \dot{m}_{4,\min} \cdot h(T_4, P_4, x_{4,id}) + \dot{m}_{7,\max} \cdot h(T_3, P_7, x_{7,id}) - \dot{m}_3 \cdot h(T_3, P_3, x_3) \quad (18)$$

If the solution is the limiting fluid ($\dot{Q}_{d,\max} = \dot{Q}_{sol,d,\max}$), the HTF imposes the temperature of the poor solution at the exit and:

$$T_4 = T_{d,i} \quad (19)$$

If instead the HTF is the limiting fluid ($\dot{Q}_{d,\max} = \dot{Q}_{HTF,d,\max}$) the HTF reaches the same temperature of the solution at the inlet ($T_{d,o} = T_3$), and the first term of Eq.(18) is equal to:

$$\dot{Q}_{d,\max} = \dot{m}_{HTF,d} \cdot cp_{HTF,d}(T_{d,i} - T_3) \quad (20)$$

The desorber thermal effectiveness is defined as the ratio between the power transferred from the HTF fluid to the solution and the maximum transferable power [29]:

$$\varepsilon_{th,d} = \frac{\dot{Q}_d}{\dot{Q}_{d,\max}} \quad (21)$$

The desorber mass effectiveness is defined as the ratio of the vapor mass flow rate generated in the desorber to the maximum vapor mass flow rate that could be generated [29]

$$\varepsilon_{mass,d} = \frac{\dot{m}_7}{\dot{m}_{7,\max}} \quad (22)$$

The desorber species effectiveness is defined as the ratio of the difference between actual ammonia and minimum ammonia concentration reachable at the outlet of the desorber, to the difference between the maximum and the minimum ammonia concentrations reachable [29]:

$$\varepsilon_{species,d} = \left(\frac{x_7 - x_{7,\min}}{x_{7,id} - x_{7,\min}}\right) \quad (23)$$

When the solution is the limiting fluid, the minimum ammonia concentration corresponds to the case in which the saturated vapor exits the desorber at the HTF inlet temperature and is calculated as:

$$x_{7,min} = x_{vap,sat}(T_{d,i}, P_3) \quad (24)$$

The energetic ratio R_{en}, number of transfer units *NTU* and Jakob number Ja are defined for the desorber as:

$$R_{en,d} = \frac{\max(\dot{Q}_{sol,d,\max}, \dot{Q}_{HTF,d,\max})}{\min(\dot{Q}_{sol,d,\max}, \dot{Q}_{HTF,d,\max})} \quad (25)$$

$$NTU_d = \frac{K \cdot S}{(\dot{m}_3 . Cp_3)} \quad (26)$$

$$Ja_d = \frac{\rho_3 . Cp_3 . (T_{d,i} - T_{3,sat})}{\rho_{vap} . L} \quad (27)$$

The desorber effectiveness were calculated for each experimental point and a correlation was found based on these three parameters using an exponential correlation similar to the ones typically used in modeling heat exchanger effectiveness [32] with the addition of the Jakob number Ja. The calculated effectiveness can vary between zero and one, asymptotically approaching this value when the magnitude of the parameters inside the exponential increases. The correlations found show that mass and thermal effectiveness have similar functions and depend mainly on the NTU and Ja. On the other hand, the species effectiveness is negatively affected by the NTU and depends mainly on the Jakob number Ja.

$$\varepsilon_{th,d} = 1 - exp(-2.285 \cdot 10^{-4} \cdot Ja_d^{1.25} \cdot NTU_d^{2} \cdot R_{en,d}^{0.66}) \quad (28)$$

$$\varepsilon_{mass,d} = 1 - exp(-3.916 \cdot 10^{-4} \cdot Ja_d^{1.33} \cdot NTU_d^{1.8} \cdot R_{en,d}^{0.6} \quad (29)$$

$$\varepsilon_{species,d} = 1 - exp(-4.774 \cdot 10^{-1} \cdot Ja_d^{1.25} \cdot NTU_d^{-0.55} \cdot R_{en,d}^{0.3}) \quad (30)$$

As shown in **Fig. 5** the effectiveness recalculated with the correlations approximate the experimental ones well, with errors below 15 % and an average error of 5.6 % for the thermal effectiveness, 7.5 % for the mass effectiveness and 2.63 % for the species effectiveness.

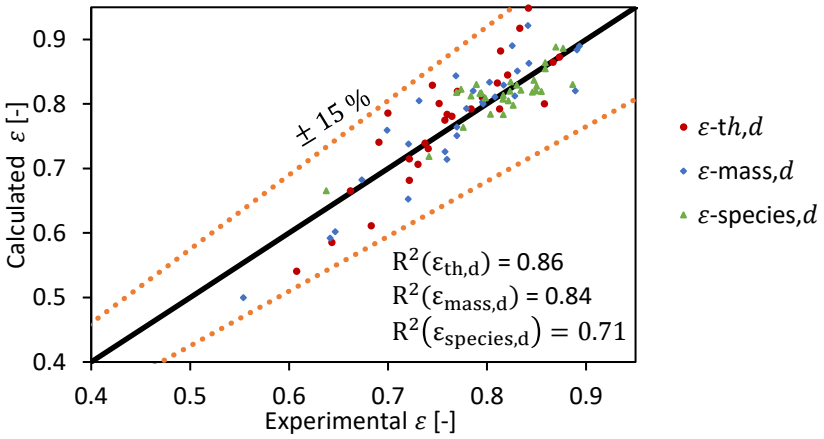

Fig. 5. Calculated desorber effectiveness vs. experimental effectiveness.

4.2.2. Absorber model

The performance of the absorber can be characterized using two effectiveness [33]: thermal effectiveness and mass effectiveness. In an ideal infinitely long absorber, after the vapor reabsorption, the solution exits from the component as saturated liquid and balance equations can therefore be written as:

$$x_{1,id} = x_{liq,sat}(T_1, P_1) \tag{31}$$

$$\dot{m}_1 = \dot{m}_{6,min} + \dot{m}_{12,max} \tag{32}$$

$$\dot{m}_1 \cdot x_{1,id} = \dot{m}_{6,min} \cdot x_{sp} + \dot{m}_{12,max} \cdot x_{ref} \tag{33}$$

$$\dot{Q}_{a,max} = \dot{m}_{7,min} \cdot h(T_6, P_6, x_6) + \dot{m}_{12,max} \cdot h(T_{12}, P_{12}, x_{12}) - \dot{m}_1 \cdot h(T_1, P_1, x_{1,id}) \tag{34}$$

If the solution is the limiting fluid ($\dot{Q}_{a,max} = \dot{Q}_{sol,a,max}$), the solution exits at the desorber HTF inlet temperature:

$$T_1 = T_{a,i} \tag{35}$$

If instead the HTF is the limiting fluid ($\dot{Q}_{a,max} = \dot{Q}_{HTF,a,max}$), the latter will reach the temperature of the poor solution entering the absorber ($T_{a,o} = T_6$) and therefore the first side of Eq. (34) will be equal to:

$$\dot{Q}_{a,max} = \dot{m}_{HTF,a} \cdot Cp_{HTF,a} \cdot (T_6 - T_{a,i}) \tag{36}$$

The absorber thermal effectiveness is defined as the ratio between the actual power transferred from the solution to the HTF fluid and the maximum transferable power in an ideal absorber.

$$\varepsilon_{th,a} = \frac{\dot{Q}_a}{\dot{Q}_{a,max}} \tag{37}$$

The absorber mass effectiveness is defined as the ratio of the absorbed vapor mass flow rate and the maximum vapor mass flow rate that could be absorbed in an ideal component [28]:

$$\varepsilon_{mass,abs} = \frac{\dot{m}_{12}}{\dot{m}_{12,max}} \tag{38}$$

The energetic ratio R_{en}, number of transfer units *NTU* and Jakob number Ja are defined for the absorber as:

$$R_{en,a} = \frac{\max(\dot{Q}_{sol,a,max}, \dot{Q}_{HTF,a,max})}{\min(\dot{Q}_{sol,a,max}, \dot{Q}_{HTF,a,max})} \tag{39}$$

$$NTU_a = \frac{K \cdot S}{(\dot{m}_1 . Cp_1)} \tag{40}$$

$$Ja_a = \frac{\rho_6 . Cp_6 . (T_{6,sat} - T_6)}{\rho_{vap} . L} \quad (41)$$

The two effectiveness are modeled based on these three parameters. The correlations found exhibit a similar dependence on the NTU as in the case of the desorber, but the R_{en} is raised to a negative power:

$$\varepsilon_{th,a} = 1 - exp\,(-9.200 \cdot 10^{-3} \cdot {Ja_a}^{0.4} \cdot {NTU_a}^{1.5} \cdot {R_{en,a}}^{-0.72}) \quad (42)$$

$$\varepsilon_{mass,a} = 1 - exp\,(-8.968 \cdot 10^{-4} \cdot {Ja_a}^{0.4} \cdot {NTU_a}^{1.5} \cdot {R_{en,a}}^{-0.92}) \quad (43)$$

The maximum error of the correlations is below 10 % for both effectiveness (**Fig. 6**), while the average error is 1.91 % for the absorber thermal effectiveness and 2.1 % for the mass effectiveness.

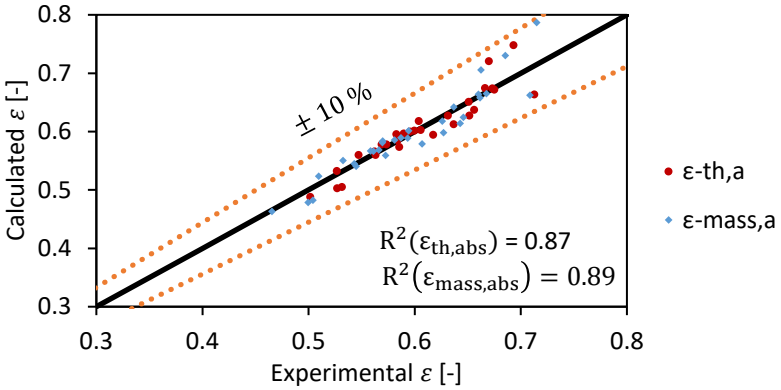

Fig. 6. Calculated absorber effectiveness vs. experimental effectiveness.

4.2.3. Other components

The evaporator being a component in which no concentration variation takes place, its functioning can be described simply using a thermal effectiveness. The maximum power that can be exchanged at the evaporator is:

$$\dot{Q}_{e,max} = \dot{m}_{11} . (h(T_{11}, P_{11}, x_{11}) - h(T_{10}, P_{10}, x_{10})) \quad (44)$$

If the solution is the limiting fluid($\dot{Q}_{e,max} = \dot{Q}_{sol,e,max}$): $T_{11} = T_{e,i}$, while if the HTF is the limiting fluid $(\dot{Q}_{e,max} = \dot{Q}_{HTF,e,max})$:

$$\dot{Q}_{e,max} = \dot{m}_{HTF,e} . (h_{HTF}(T_{e,i}, P_{HTF}) - h_{HTF}(T_{10}, P_{HTF})) \quad (45)$$

The evaporator thermal effectiveness is defined as the ratio between the actual power transferred from the HTF fluid to the solution to the maximum transferable power.

$$\varepsilon_{th,e} = \frac{\dot{Q}_e}{\dot{Q}_{e,max}} \quad (46)$$

The evaporator effectiveness is modeled well using R_{en} and NTU defined as:

$$R_{en,e} = \frac{\max(\dot{Q}_{sol,e,max}, \dot{Q}_{HTF,e,max})}{\min(\dot{Q}_{sol,e,max}, \dot{Q}_{HTF,e,max})} \quad (47)$$

$$NTU_e = \frac{K \cdot S}{(\dot{m}_{13} . Cp_{13})} \quad (48)$$

The correlation found for the thermal effectiveness of the evaporator depends mainly on the R_{en} while the NTU is raised to a relatively smaller power.

$$\varepsilon_{th,e} = 1 - exp\,(-1.231 \cdot {NTU_e}^{0.25} \cdot {R_{en,e}}^{0.8}) \quad (49)$$

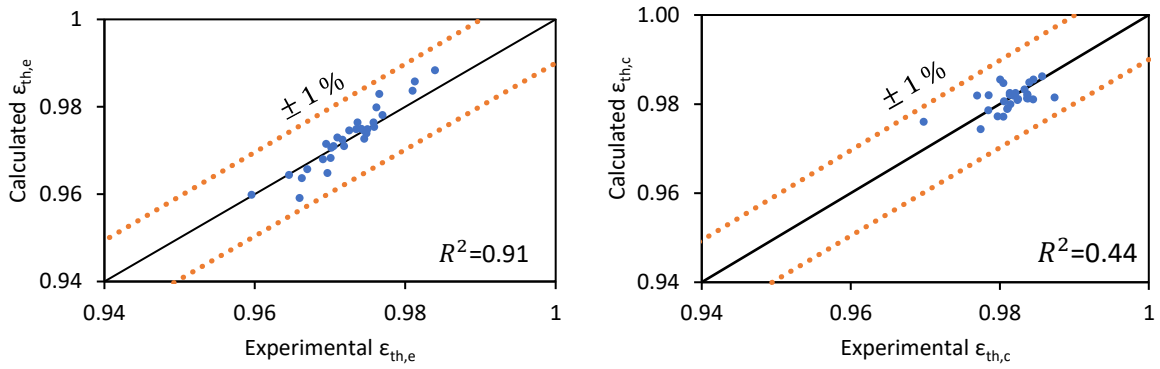

Fig. 7. Calculated evaporator and condenser effectiveness vs. experimental effectiveness.

As for the case of the evaporator, the condenser is also described well using just a thermal effectiveness function of R_{en} and NTU. Therefore, an identical method can be applied in the case of the condenser, leading to the following correlation:

$$\varepsilon_{th,c} = 1 - exp\,(-1.930 \cdot {NTU_c}^{0.1} \cdot {R_{en,c}}^{0.2}) \tag{50}$$

The correlation found for the thermal effectiveness of the condenser reveals the small value of the powers to which both NTU and R_{en} are raised in accordance with the small variance of this effectiveness. The maximum error of the correlations is below 1 % for both the evaporator and condenser thermal effectiveness while the average error is 0.2 % and 0.25 % respectively as shown in **Fig. 7**.
Equivalent thermal effectiveness can also be defined for the two internal heat exchangers, the solution heat exchanger and the subcooler.

$$\varepsilon_{th,shx} = 1 - exp\,(-0.4066 \cdot {NTU_{shx}}^{0.5} \cdot {R_{en,shx}}^{1.03}) \tag{51}$$
$$\varepsilon_{th,sub} = 1 - exp\,(-0.0736 \cdot {NTU_{sub}}^{1.77} \cdot {R_{en,sub}}^{2.25}) \tag{52}$$

The maximum error of the correlation with respect to the experimentally calculated effectiveness is below 5 % for the solution heat exchanger and below 3 % for the subcooler, with an average error below 1.2 and 0.9 % respectively as shown in **Fig. 8**.

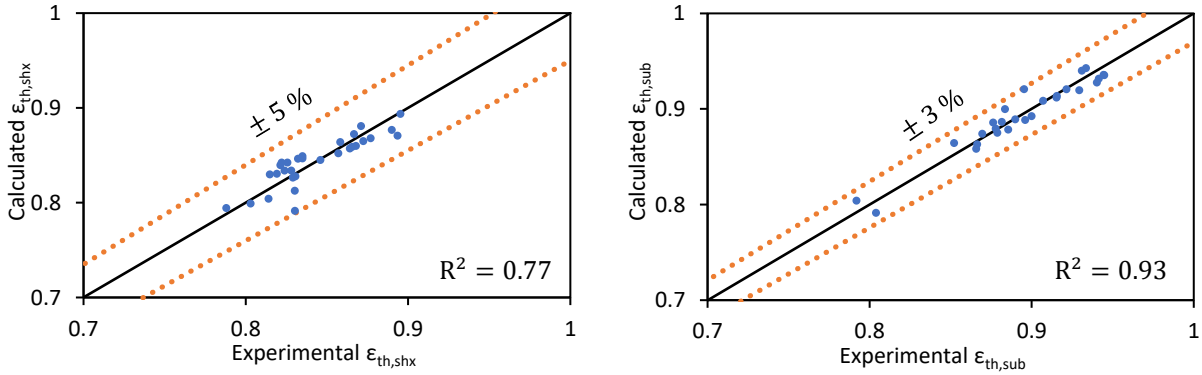

Fig. 8. Calculated solution heat exchanger and subcooler effectiveness vs. experimental effectiveness.

4.2.4. Alternative thermal effectiveness modeling

An alternative to the use of the thermal effectiveness presented in the previous sections is to model for each exchanger the ΔT between the two fluids. This can be especially useful in cases where due to the limited variability of experimental conditions the range of variation of the thermal effectiveness is very small. In particular, this is the case for the condenser where the range of variation of the thermal effectiveness is smaller than 1.7 %. In addition, the temperature pinch between the solution and the HTF on the condenser and on the evaporator is a very important parameter defining the high and low pressure of the cycle respectively. Therefore, in the case of the condenser this second type of modeling for the thermal effectiveness was preferred.

The correlation found for the condenser pinch of temperature $\Delta T_c = T_8 - T_{c,i}$ as a function of $\Delta T_{c,max} = T_7 - T_{c,i}$, $R_{en,c}$ and NTU_c is :

$$\Delta T_c = \Delta T_{c,max} \cdot \exp(-0.65 \cdot {R_{en,c}}^{0.4} \cdot {NTU_c}^{0.1}) \quad (53)$$

Knowing ΔT_c, $\varepsilon_{th,c}$ can be calculated as follows:

$$\varepsilon_{th,c} = \frac{\dot{m}_{ref} \cdot (h(T_9, P_9, x_{ref}) - h(T_{11}, P_{11}, x_{ref}))}{\dot{Q}_{c,max}} \quad (54)$$

Where $T_8 = T_{ci} + \Delta T_c$.

The average and maximum error for the ΔT_c were 2.2% and 5 % (**Fig. 9)**, while the average error for the $\varepsilon_{th,e}$ calculated through the use of ΔT_c was 0.27 %.

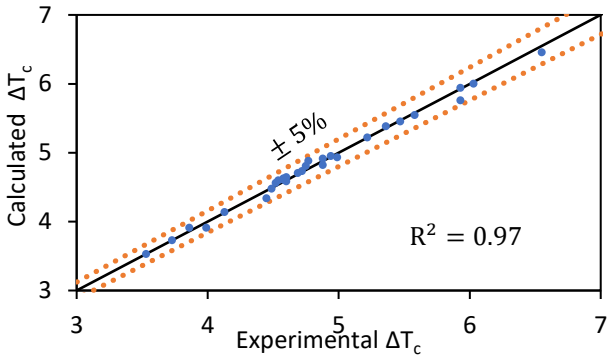

Fig. 9. Calculated vs. experimental ΔT_c and derived $\varepsilon_{th,c}$

4.3. Comparison of the simplified and effectiveness *models*

The correlations for the component effectiveness modeled in the previous sections are implemented in the numerical model of the cycle. The comparison of the ε-model results to the experimental data (**Fig. 10**) shows that the model predicts the performance of the machines very well both in terms of COP and cooling power output with errors below 6 % for the COP and 15 % for the cooling power.

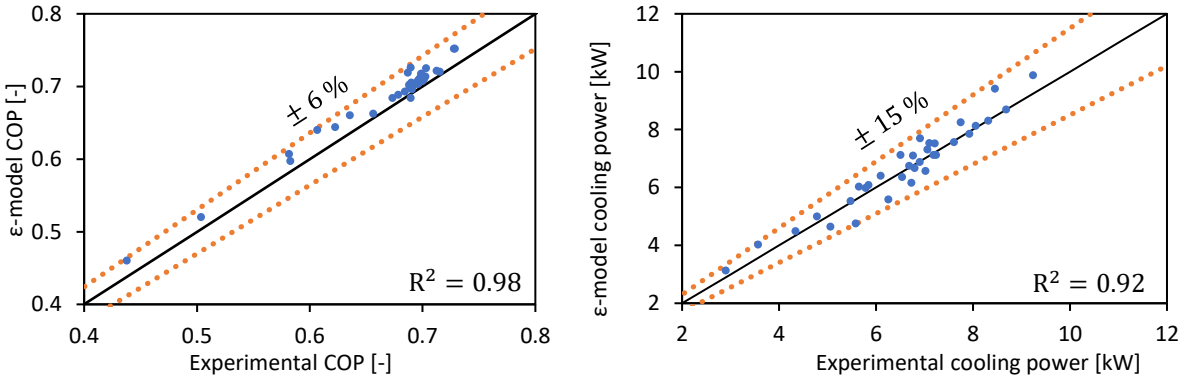

Fig. 10. Effectiveness model results compared to experimental results.

Table 6 compares the average and maximum error of the effectiveness model with those of the simplified model presented in Section 4.1. It is evident that the effectiveness model improves the accuracy of the predicted cycle performance significantly with an average error compared to experimental results of only 2.4 % for the COP and 5.4 % for the cooling power output, against 6.3 % and 12.5 % average error respectively in the case of the simplified model. Even more remarkable is the improvement in the maximum error, which was reduced from 50 % to 5.5 % for the COP and from 65 % to 14.8 % for the cooling power output.

Table 6

Simplified model and effectiveness model error compared to experimental data.

	Simplified model		Effectiveness model	
	COP	Cooling power output	COP	Cooling power output
Average Error	6.3 %	12.5 %	2.4 %	5.4 %
Maximum Error	50 %	65 %	5.5 %	14.8 %
R^2	0.39	0.70	0.98	0.92

Fig. 11 compares the performance calculated by the simplified and the ε-model at the same points of **Table 5** where only one parameter at a time is changed while the others are left constant at nominal conditions (**Table 4**).

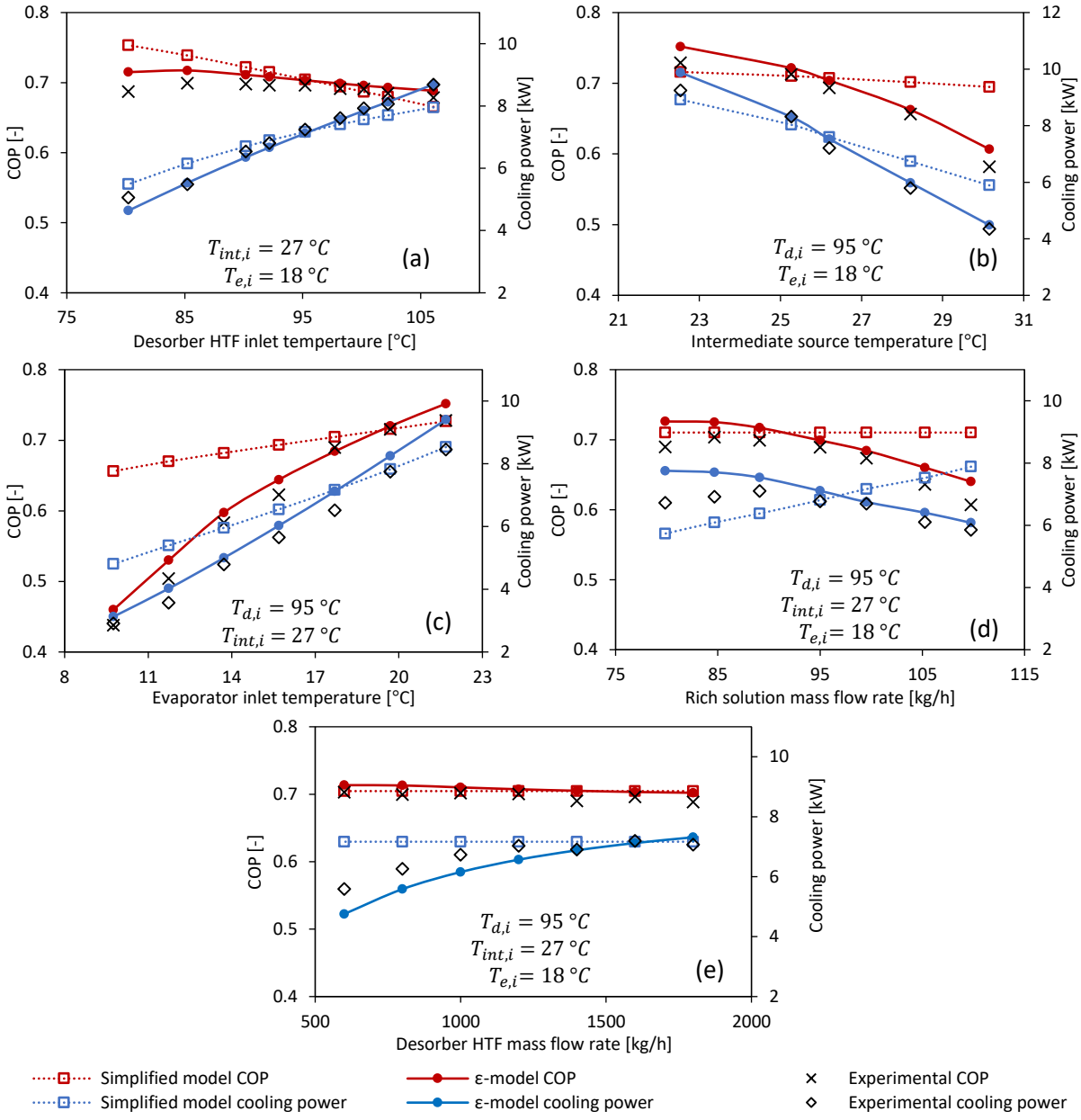

Fig. 11. Simplified model and ε-model results compared to experimental results.

Fig. 11(a) shows that, as expected, the cooling power produced $\dot{Q}_e$ strongly increases when the desorber inlet temperature $T_{d,i}$ increases reaching up to 9 kW at 106°C, while the influence of $T_{d,i}$ on COP appears to be more limited with an optimum of 0.72 around 80°C. Higher desorber inlet temperatures increase the thermal

effectiveness of the component and thus the mass flow rate of desorbed vapor, thus increasing the cooling production of the cycle, despite the slight COP decreases due to the reduced purification capacity of the desorber (i.e. species effectiveness) when the hot source temperature increases. The COP and $\dot{Q}_e$ predicted by the simplified model are accurate near the nominal working conditions where the results are very similar to those of the ε-model. Nevertheless, given that fixed effectiveness and ΔT are used for all operating points, the simplified model fails to predict the variation of performance found with variation of both the intermediate source and the evaporator inlet temperature. In fact, **Fig. 11(b)** shows that in the case of the simplified model the COP is only slightly affected by the intermediate source temperature while instead, in accordance with experimental results, the COP decreases noticeably in the case of the ε-model from 0.75 at 23 °C to 0.6 at 30 °C. The difference found when decreasing the evaporator inlet temperature appears to be even more significant **Fig. 11(c)**, which reduces the COP from over 0.7 at 21 °C to 0.45 at 10 °C for the ε-model, while only a much smaller performance decrease is predicted by the simplified model. In addition, the simplified model does not take into account the geometry of the exchangers and therefore, in contrast with the experimental results, the mass flow rate of solution has no effect on COP and linearly increases $\dot{Q}_e$ **Fig. 11(d)**. Results of the adjusted effectiveness model show instead a performance decrease when the solution mass flow rate increases with an optimum of around 85 kg/h. Finally, side fluid is not considered in the simplified model and therefore it has no influence on the behavior of the machine, as opposed to the effectiveness model which considers this. As an example, **Fig. 11(e)** shows that reducing the desorber HTF has little effect on the COP but strongly reduces the cooling power output.

5. Parametric study of the size of components

The model developed contains information about the geometry of the components, making it possible to perform parametric analysis on their size to study its influence on global performance of the cycle. **Fig. 12** shows the impact on cycle performance of doubling or halving the size of the absorber for different intermediate and evaporator temperatures at the nominal desorber conditions and solution mass flow rate. (**Table 4)**. The absorber is a bottleneck component [31] and reducing its size by half compared with the base case presented in **Table 2** generates an average COP and $\dot{Q}_e$ output reduction of 31 % and 57 % respectively. In addition, significant performance improvements are possible by increasing its size. For example, doubling the size of the absorber leads to an average increase in the COP of 14 % and in the cooling power of 41 %. Additionally, the impact of the absorber size on COP is higher at evaporator temperatures lower than design conditions, where the component operates at lower pressure and thus less efficiently. On the other hand, in the nominal operating point, increasing the size of the absorber has a smaller impact, since the absorber base size was designed to guarantee good performance in that point.

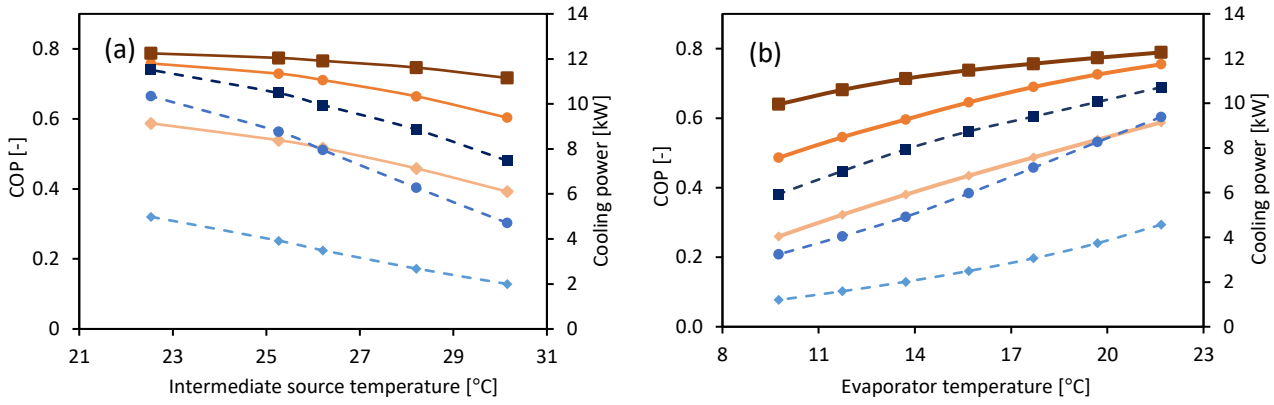

Fig. 12. Change of COP [-] (orange symbols, bold line) and cooling power [kW] (blue symbols, dotted line) as a function of the intermediate temperature (a), evaporator temperature (b) and absorber size (● = base size, ■ = double size, ◆ = half size) for nominal desorber conditions and solution mass flow rate.

The results of the analysis carried out for the evaporator are shown in **Fig. 13Erreur ! Source du renvoi introuvable.**. In this case a reduction in the size of the evaporator also generates an average reduction of 9 % in the COP and 22 % in the cooling power output. Doubling the size of the evaporator instead leads on average to a 5.5 % increase in the COP and 17 % in the cooling output.

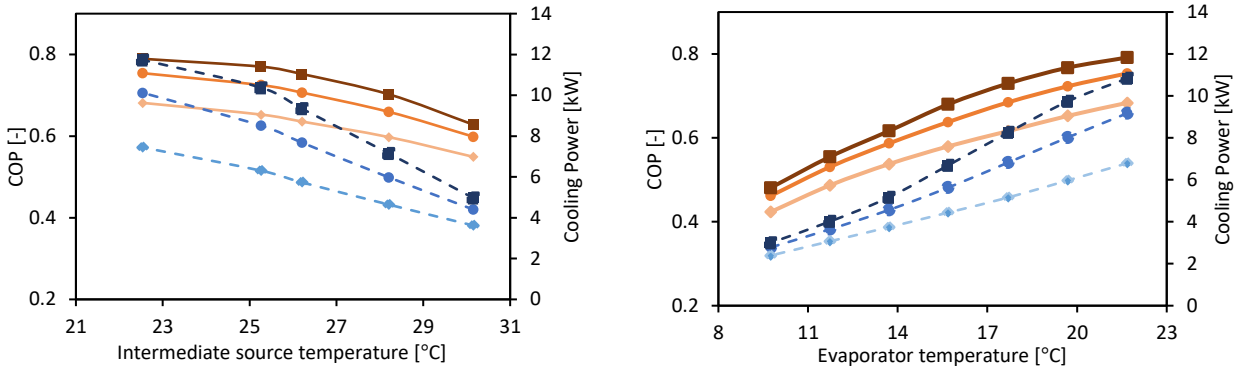

Fig. 13. Change of COP [-] (orange symbols, bold line) and cooling power [kW] (blue symbols, dotted line) as a function of the intermediate temperature (a), evaporator temperature (b) and evaporator size (● = base size, ■ = double size, ◆ = half size) for nominal desorber conditions and solution mass flow rate.

The effect of the size of the desorber on cycle performance is different, as shown in **Fig. 14**. In fact, an increase in size has a positive effect on cooling power output, with an average $\dot{Q}_e$ increase of 18 % for a desorber of double the size and a 44 % decrease on average for a desorber of half the size. The same is not true for the COP of the cycle which does not always increase with the size of the desorber. This is because a larger desorber enables the transfer of more power to the solution and to the desorbed vapor ($\varepsilon_{th,d}$ increases with the NTU in Eq.(28)) which will be hotter and produced at higher mass flow rates. This influences the internal rectification process in the adiabatic part of the desorber increasing the ΔT between the exiting vapor and the solution at inlet. The ability to purify the refrigerant vapor is therefore reduced as confirmed by the negative power to which the NTU is raised in the correlation for $\varepsilon_{species,d}$ in Eq.(30). Imperfect vapor purification can have a very negative impact on COP suggesting the need for increasing the solution mass flow rate or adding a rectifier to further purify the vapor when the desorber size is increased.

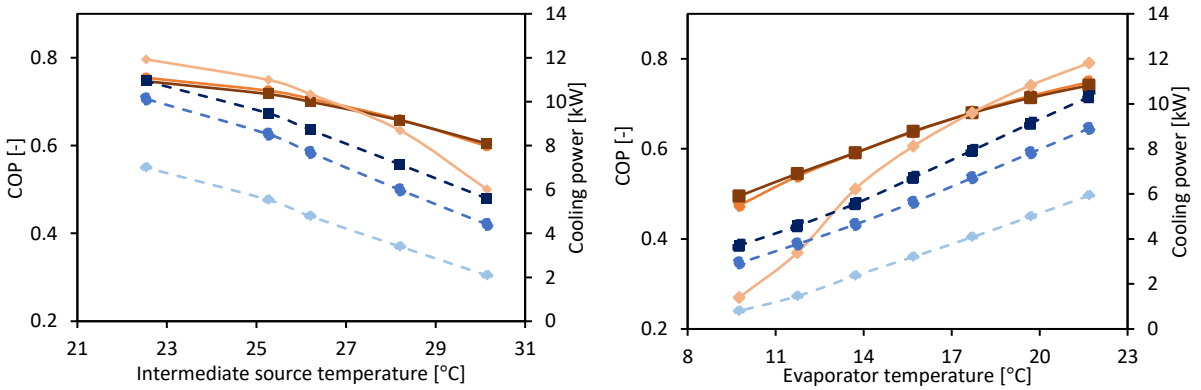

Fig. 14. Change of COP [-] (orange symbols, bold line) and cooling power [kW] (blue symbols, dotted line) as a function of the intermediate temperature (a), evaporator temperature (b) and desorber size (● = base size, ■ = double size, ◆ = half size) for nominal desorber conditions and solution mass flow rate.

Finally, the condenser was found to have a smaller impact on performance: doubling the condenser size leads to an average improvement of 3 % in the COP and 12 % in the cooling power while a condenser of half the size reduced the COP by 5 % on average and the cooling power output by 16 %. **Table 7** summarizes the effect on performance of the size of the components in the range of operation considered. The results are due to the intrinsic criticality of the components in the cycle. Components where heat and mass transfers take place at the same time (the desorber and even more the absorber), are the most crucial ones in absorption machines and particular attention needs to be paid to their design. It should be highlighted that the results of the parametric analysis also depend on the base size of the pilot plant components. The possibility of performing such studies on the size of components can be very useful in the design phase and when performing techno-economic or thermo-economic analysis of the technology.

Table 7
Influence of the size of components on cycle performance and cooling production for variation of the intermediate source temperature [22-30 °C] and evaporator temperature [10-22 °C] around the nominal point.

	Double Size		Half Size	
	COP	Cooling Power	COP	Cooling Power
Absorber	+ 17 %	+ 51 %	- 30 %	- 54 %
Desorber	+ 0.14 %	+ 18 %	- 7.6 %	- 45 %
Evaporator	+ 5.5 %	+ 17 %	- 9 %	- 22 %
Condenser	+ 3 %	+ 12 %	- 5 %	- 16 %

6. Conclusions

Absorption machines represent an alternative to conventional vapor compression systems for their ability to use renewable energy sources and waste energy. Therefore, expanding their use could help reduce greenhouse gas emissions as well as electricity consumption. Nevertheless, these systems are still more costly and complex than traditional systems and need to be developed further. Appropriate modeling is fundamental to their performance characterization and optimization.

An experimental campaign on a 7 kW cooling power ammonia-water absorption chiller was carried out to create an accurate database for the numerical model adjustment. Experimental results were analyzed critically to obtain all the necessary thermo-physical properties, and unreliable points were excluded from further analysis. First, a simplified model based on fixed pinch points and absorber mass effectiveness estimated from experimental tests was developed. The model provided good results at the design point of operation but did not sufficiently describe the behavior of the machine under different conditions thus preventing generalization of the results at larger scales and with more complex architectures.

Therefore, another model was developed based on thermal, mass, and species effectiveness relating the functioning of components to that of ideal ones. Experimental measures were used to characterize the effectiveness of the components in different operating conditions and correlations were found to model them based on three dimensionless parameters: the Jakob number *Ja*, the energetic ratio R_{en} and the number of transfer units *NTU*. The model integrating correlations for each component showed very good agreement with experimental results, with a maximum error below 6 % for the COP and 15 % for the cooling power output. Results confirm a cooling power output of around 7 kW and a COP of 0.7 in nominal conditions of 95 °C of high temperature source, 27 °C intermediate temperature and 18 °C of evaporator inlet temperature.

The tuned model was used to perform a parametric analysis on the dimension of the components, highlighting the absorber, the desorber and the evaporator to be the most critical components of the pilot plant and therefore those with the greatest room for improvement. The use of dimensionless parameters makes this approach well suited for analysis at larger scales of industrial interest and for the development of more complex combined cycles. Nevertheless, further experimental studies are necessary to confirm the validity of the model for different plant sizes and architectures.

Declaration of Competing Interest

The authors declare that they have no known competing financial interests or personal relationships that could have appeared to influence the work reported in this paper.

Acknowledgements
The authors would like to express their gratitude to the French Alternative Energies and Atomic Energy Commission and the Carnot Energies of the Future Institute. S. Braccio was supported by the CEA NUMERICS program, which has received funding from the European Union's Horizon 2020 research and innovation program under the Marie Sklodowska-Curie grant agreement No 800945.

7. References

[1] Http://mission-innovation.net/, Mission Innovation, (2020).

[2] European Commission, Clean energy for all Europeans, Euroheat Power (English Ed. (2019). https://doi.org/10.2833/9937.

[3] M. Ragwitz, A. Herbst, S. Hirzel, M. Ragwitz, M. Rehfeldt, M. Reuter, J. Steinbach, EUROPEAN COMMISSION DIRECTORATE-GENERAL FOR ENERGY Directorate C. 2 – New energy technologies, innovation and clean coal, (n.d.).

[4] D. 2017 DG Energy, The Strategic Energy Technology (SET) Plan - At the heart of energy research and innovation in Europe-European Commission Directorate-General for Research and Innovation, 2017.

[5] International Renewable Energy Agency (IRENA), Global energy transformation: A roadmap to 2050 (2019 edition), ISBN 978-92-9260-121-8. (2019).

[6] F. Birol, The Future of Cooling-Opportunities for energy efficient air conditioning- Opportunities for energy efficient air conditioning, OECD/IEA 2018. (2018).

[7] K.E. Herold, R. Radermacher, S.A. Klein, Absorption Chillers and Heat Pumps, 2016. https://doi.org/10.1201/b19625.

[8] S. Aphornratana, S. Chungpaibulpatana, P. Srikhirin, Experimental investigation of an ejector refrigerator: Effect of mixing chamber geometry on system performance, Int. J. Energy Res. (2001). https://doi.org/10.1002/er.689.

[9] P. Srikhirin, S. Aphornratana, S. Chungpaibulpatana, A review of absorption refrigeration technologies, Renew. Sustain. Energy Rev. (2000). https://doi.org/10.1016/S1364-0321(01)00003-X.

[10] K.R. Ullah, R. Saidur, H.W. Ping, R.K. Akikur, N.H. Shuvo, A review of solar thermal refrigeration and cooling methods, Renew. Sustain. Energy Rev. (2013). https://doi.org/10.1016/j.rser.2013.03.024.

[11] A. Altamirano, N. Le Pierrès, B. Stutz, Review of small-capacity single-stage continuous absorption systems operating on binary working fluids for cooling: Theoretical, experimental and commercial cycles, Int. J. Refrig. 106 (2019) 350–373. https://doi.org/10.1016/j.ijrefrig.2019.06.033.

[12] S. Braccio, H.T. Phan, N. Tauveron, Study of a cold and electric cogeneration machine using a low temperature heat source., SFT 2021. (2021). https://doi.org/https://doi.org/10.25855/SFT2021-036.

[13] F. Boudéhenn, H. Demasles, J. Wyttenbach, X. Jobard, D. Chèze, P. Papillon, Development of a 5 kW cooling capacity ammonia-water absorption chiller for solar cooling applications, Energy Procedia. 30 (2012) 35–43. https://doi.org/10.1016/j.egypro.2012.11.006.

[14] S. Braccio, H.T. Phan, N. Tauveron, N. Le Pierrès, Study of the integration of a supersonic impulse turbine in a NH 3 / H 2 O absorption heat pump for combined cooling and power production from a low temperature heat source , E3S Web Conf. 312 (2021) 08018. https://doi.org/10.1051/e3sconf/202131208018.

[15] F. Boudéhenn, S. Bonnot, H. Demasles, A. Lazrak, Comparison of Different Modeling Methods for a Single Effect Water-Lithium Bromide Absorption Chiller, (2015) 1–10. https://doi.org/10.18086/eurosun.2014.07.04.

[16] A. Altamirano, N. Le Pierrès, B. Stutz, A. Coronas, Performance characterization methods for absorption chillers applied to an NH3-LiNO3 single-stage prototype, Appl. Therm. Eng. 185 (2021). https://doi.org/10.1016/j.applthermaleng.2020.116435.

[17] J. Labus, J.C. Bruno, A. Coronas, Performance analysis of small capacity absorption chillers by using different modeling methods, Appl. Therm. Eng. 58 (2013) 305–313. https://doi.org/10.1016/j.applthermaleng.2013.04.032.

[18] J.M. Gordon, K.C. Ng, A general thermodynamic model for absorption chillers: Theory and experiment, Heat Recover. Syst. CHP. 15 (1995) 73–83. https://doi.org/10.1016/0890-4332(95)90038-1.

[19] C. Ziegler, F., Hellmann, H.M., Schweigler, An approximative method for modeling the operating characteristics of advanced absorption chillers., in: Int. Congr. Refrig., Sydney, Autralia., n.d.

[20] E. Thorin, Comparison of correlations for predicting thermodynamic properties of ammonia-water mixtures, Int. J. Thermophys. 21 (2000) 853–870. https://doi.org/10.1023/A:1006658107014.

[21] S.S. Stecco, U. Desideri, A thermodynamic analysis of the Kalina cycles: Comparisons, problems and perspectives, Proc. ASME Turbo Expo. 4 (1989). https://doi.org/10.1115/89GT-149.

[22] S.A. Ibrahim, O.M., Klein, Thermodynamic properties of ammonia-water mixtures., in: ASHRAE Trans. Symp. 21, 2, 1495, n.d.

[23] R. Tillner-Roth, D.G. Friend, A Helmholtz free energy formulation of the thermodynamic properties of the mixture {water + ammonia}, J. Phys. Chem. Ref. Data. 27 (1998) 63–77. https://doi.org/10.1063/1.556015.

[24] J. Dardouch, M. Charia, A. Bernatchou, Study of an absorption refrigeration machine improved with distillation column, J Mater Env. 9 (2018) 772–783.

[25] M. Wirtz, B. Stutz, H.T. Phan, F. Boudehenn, Numerical modeling of falling-film plate generator and rectifier designed for NH3—H2O absorption machines, Heat Mass Transf. (2021). https://doi.org/10.1007/s00231-021-03111-z.

[26] M. Wirtz, B. Stutz, H.T. Phan, F. Boudéhenn, Numerical modeling and integration of a falling film plate generator/rectifier in a NH3/H2O absorption machine prototype, in: SFT 2021, Belfort, 2021: pp. 369–376. https://doi.org/https://doi.org/10.25855/SFT2021-011.

[27] M.A. Staedter, S. Garimella, Direct-coupled desorption for small capacity ammonia-water absorption systems, Int. J. Heat Mass Transf. 127 (2018) 196–205. https://doi.org/10.1016/j.ijheatmasstransfer.2018.06.118.

[28] D. Triché, S. Bonnot, M. Perier-Muzet, F. Boudéhenn, H. Demasles, N. Caney, Experimental and numerical study of a falling film absorber in an ammonia-water absorption chiller, Int. J. Heat Mass Transf. 111 (2017) 374–385. https://doi.org/10.1016/j.ijheatmasstransfer.2017.04.008.

[29] M. Wirtz, Development of a falling-film desorber combining vapor generation and purification for ammonia–water absorption chiller (Modeling and Experiments), PhD Thesis, Université Savoie Mont Blanc, 24th February 2022.

[30] F.P. Incropera, Fundamentals of Heat and Mass Transfer, John Wiley & Sons, Inc., Hoboken, NJ, USA, 2006.

[31] D. Triche, Numerical and experimental study of coupled mass and heat transfers in the absorber of an ammonia-water absorption chiller, 2016. https://tel.archives-ouvertes.fr/tel-01696252.

[32] Y.A. Cengel, Introduction to Thermodynamics and Heat Transfer 2nd Edition, Ther. Hypothermia. (2004) 265–292.

[33] M. Perier-Muzet, B. Stutz, Numerical study of the effectiveness of a vertical falling plate film absorber for an absorption chiller, Int. J. Refrig. 127 (2021) 221–229. https://doi.org/10.1016/j.ijrefrig.2021.02.013.